Engineering

Mechanical Engineering fields

Okayama University *Year* 2007

Sublimation Behavior of Annular Frost Layer by Impinging Jet Flow

Hideo Inaba[*] Akihiko Horibe[†] Naoki Takamoto[‡]
Yoshiaki Kawakami[**] Seishi Imai[††]

[*]Okayama University
[†]Okayama University
[‡]Okayama University
[**]Okayama University
[††]Coil Division, Matsushita Refrigeration Co., Ltd

Sublimation Behavior of Annular Frost Layer by Impinging Jet Flow*

Hideo INABA**, Akihiko HORIBE**,
Naoki TAKAMOTO**, Yoshiaki KAWAKAMI**
and Seishi IMAI***

The present paper deals with a new method of defrosting using the frost sublimation phenomenon, which occurs below the triple point of water (273.16 K, 610.5 Pa). The present experimental study examines the mass transfer of the annular frost layer developed on a cooling pipe exposed to an impinging jet flow. The morphology of the frost layer during sublimation was observed using a digital video recorder. It was understood that the mass flux of the frost layer increased with increasing the jet flow velocity and the difference in the mass concentration of water vapor between the frost surface and the impinging jet flow. The non-dimensional correlation equations of mass transfer of defrosting were derived as functions of various parameters.

Key Words: Defrost, Frost Layer, Impinging Jet Flow, Sublimation, Mass Transfer

1. Introduction

A frost layer developed on a cooling surface of a cold heat exchanger results in a decrease in heat transfer and an increase in blower power due to a decrease in the sectional area of the air flow pass. Therefore, a great deal of attention has been paid to the development of new effective defrosting methods.

Some conventional methods have been used for defrosting such as the frost melting methods by hot gas in a reverse refrigerating cycle and an electric heater. These common methods, however, result in a decrease in the cooling function and thermal efficiency because of the interruption of the refrigeration cycle, an economical disadvantage owing to the small ratio of the energy consumed to melt the frost layer to the total energy supplied during the defrosting process (approximately 20%[1]), and the treatment problem of melted water.

In general, ice sublimates from solid to water vapor below the triple point of water (273.16 K). Using the sublimation for defrosting, the melted water does not remain on a cooling surface because the frost becomes water vapor directly which diffuses into the air. In addition, frost sublimation makes the defrosting possible when the temperature of the heat exchanger remains low, because it occurs on the surface of the frost layer. A number of investigations of sublimation characteristics have been carried out. Kumada et al.[2] have measured the local heat transfer coefficients around a pipe by the naphthalene sublimation method. To provide information for freeze-drying, which is the one of the preservation methods of food that uses sublimation of ice, Kochs et al.[3] have reported a sublimation rate under various conditions in the case of natural convection. Furthermore, two of the current authors[4]-[6] have examined the sublimation characteristics of the horizontal frost layer in the forced convection that flowed parallel or vertically with respect to the frost layer.

The present study was performed to examine the sublimation behavior of the frost layer with a view to utilizing the sublimation phenomenon for defrosting of the frost layer developed on a common tube-type

* Received 22nd October, 2001. Japanese original: Trans. Jpn. Soc. Mech. Eng., Vol. 66, No. 650, B (2000), pp. 2661-2668 (Received 16th December, 1999)

** Okayama University, Graduate School of National Science and Technology, 3-1-1 Tsushimanaka, Okayama-city 700-8530, Japan. E-mail: inaba@mech.okayama-u.ac.jp

*** Coil Division, Matsushita Refrigeration Co., Ltd., Japan, Nozityou 2275, Kusatsu-city 525-0055, Japan

cold-heat exchanger. In this study, a jet flow of cold air, which was blown from a two-dimensional nozzle, was impinged against the annular frost layer developed on a pipe to promote sublimation. The experiments were carried out to determine the effects of the experimental parameters such as jet flow temperature and velocity at the nozzle outlet, distance between nozzle and frost layer surface, water-vapor mass concentration of the jet flow, initial frost height, and initial frost density on defrosting characteristics by sublimation from the frost layer.

2. Nomenclature

a : thermal diffusivity of frost layer, mm²/s
B : width of nozzle, mm
C_∞ : water-vapor mass concentration of jet flow, g/m³
C_s : saturated water-vapor mass concentration at a frost layer temperature, g/m³
C_p : specific heat at constant pressure of air, kJ/kg
D : diffusion coefficient of air, m²/s
d : test pipe diameter, mm
d_f : representative length ($d+2H_f$), mm
Gu : Guman number
H : distance between nozzle and frost layer surface, mm
h_D : mass transfer coefficient, m/s
H_f : initial frost height, mm
L : sublimation latent heat of ice, kJ/kg
l : test pipe length, mm
M_f : mass of frost layer, g
M_s : sublimation quantity, g
m_{Af} : sublimation mass flux, kg/(m²•s)
Q_{cv} : amount of convection heat, W
Q_s : amount of sublimation latent heat, W
Q_f : amount of sensible heat of frost layer, W
Q_p : amount of sensible heat of test pipe, W
Re_B : Reynolds number at nozzle outlet of jet flow
S : apparent sublimation area, m²
Sc : Schmidt number
Sh : Sherwood number
T_a : attainment temperature of jet flow, K
T_p : mean temperature of test pipe surface, K
T_{TP} : temperature at triple point of water, K
T_∞ : jet flow temperature at nozzle outlet
U_B : velocity of jet flow at nozzle outlet, m/s
δ : thickness of test pipe, mm
ϕ_∞ : relative humidity, %
ρ_f : initial density of frost layer, kg/m³
ρ_{ice} : density of ice, kg/m³
ρ^* : density ratio
λ : thermal conductivity of jet flow, W/(m•K)
ν : kinematic viscosity of jet air, m²/s
θ : angle from upper stagnation point, °

Subscripts
0 : exposure of stagnation point
c : completion of defrosting
f : frost layer
p : test pipe
s : sublimation
∞ : nozzle outlet

3. Experimental Apparatus and Procedures

Figure 1 shows the experimental apparatus used in the present study, which was set in an air-conditioned room. The temperature of the flowing moist air was carefully controlled in the range from 15°C to −20°C by a refrigerator and electric heaters. The humidity of the moist air was also controlled by means of a membrane dryer and a humidifier. The air, which was maintained at the designated temperature and humidity values, was supplied to a pressure chamber made of acrylic resin plates by a variable inverter blower (max. pressure 2.1 kPa, quantity of air flow 0.5 ~ 2.0 m³/min.). Figure 2 indicates the details of the test section. The impinging jet flow was formed by air blowing from a two-dimensional nozzle mounted on the bottom of the pressure chamber. The two-dimensional nozzle has a rectangular cross-sectional area B=4.0 mm wide and 400 mm long, which consisted of a semi-circular part 15.0 mm in radius and parallel part 5.0 mm thick as shown in the upper part of Fig. 2. The temperature of the jet flow was measured with T-type thermocouples of 0.3 mm diameter (measurement accuracy of ±0.1°C) at the nozzle outlet. The water-vapor mass concentration of the jet

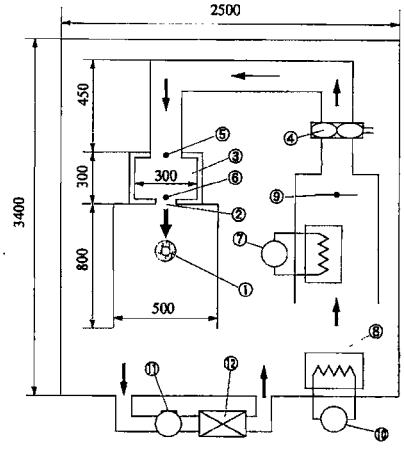

① Frost layer, ② Nozzle, ③ Pressure chamber, ④ Blower, ⑤ Humidity sensor, ⑥ Thermocouple, ⑦ Electric heater, ⑨ Heat exchanger, ⑨ Damper, ⑩ Refrigerator, ⑪ Membrane dryer, ⑫ Compressor

Fig. 1 Schematic diagram of experimental apparatus

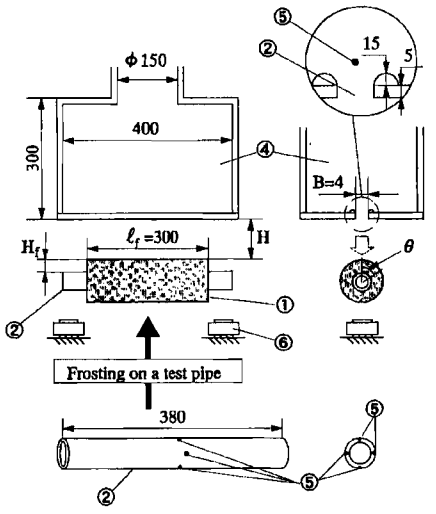

① Frost layer, ② Test pipe, ③ Nozzle, ④ Pressure chamber, ⑤ Thermocouple, ⑥ Electric balancer

Fig. 2 Details of test section

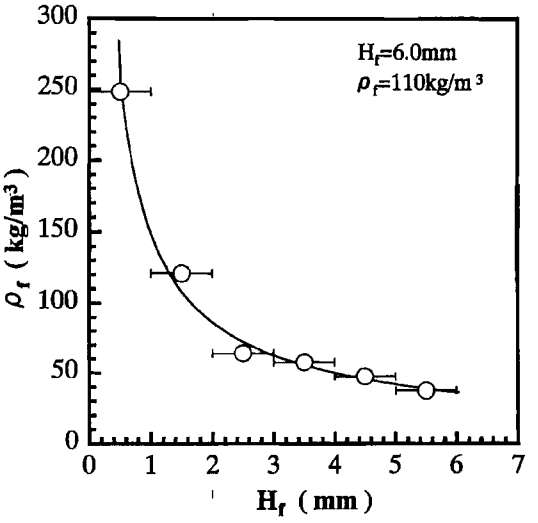

Fig. 3 Vertical density distribution in a frost layer

flow C_∞ was calculated with both the jet flow temperature and the dew-point temperature of the jet flow which was measured with a chilled mirror dew-point hygrometer (measuring accuracy of ±0.1°C). The distance between the nozzle and the frost layer surface H could be set to the prescribed distance in the range from 8 mm to 80 mm. Generally, a decrease in the distance H causes the flow pattern of the jet flow to vary from the fully developed jet region, and pass through transition region to the potential core region[7].

In the present experiment, the test pipe was made of a copper tube, which had dimensions of 19.05 mm outer diameter d, 380 mm length l, and 0.8 mm thickness δ. Four T-type thermocouples of 0.1 mm diameter (measurement accuracy of ±0.1°C) were mounted around the pipe surface to measure the temperature at intervals of 90 deg. including the stagnation point (θ= 0 deg.). Leads of the thermocouples were fixed in the grooves on the pipe surface with epoxy resin, after that, the pipe surface was carefully made smooth.

The frost layer as a test sample for defrosting was accumulated on the test pipe in the air-conditioned room by using cold brine flowing in the pipe. The frost layer had a length of l_f=300 mm, while initial frost height H_f could be controlled at the designated value. The initial frost height H_f was defined by the mean height from the pipe surface to the top of the frost layer, which was calculated with the data at eight measurement points at intervals of 45 deg in the pipe circumference direction and four points in the pipe length direction. H_f was measured with a vernier caliper (measuring accuracy of ±0.05 mm) and from the photograph of the frost layer, which was magnified approximately three times. Considering the error of measurement, the uncertainty of H_f was estimated to be about ±0.1 mm. On the other hand, the initial density of the frost layer ρ_f was calculated with the initial mass of the frost layer divided by its apparent volume. In this experiment, the density and height of the frost layer could be controlled at the designated values by the adjustment of the time period for frosting under the conditions at the test pipe surface temperature: −30 ~ −15°C, and circumference temperature: −10 ~ −2°C. Figure 3 shows the vertical density distribution in the frost layer (initial height H_f=6.0 mm). The density distribution was obtained from the mass and apparent volume of each thin frost layer that was sliced to a 1 mm thickness from the top of the frost layer to the bottom. As shown in Fig. 3, there was a decrease in density at the top of the frost layer compared to the bottom.

The defrosting experiments were carried out using the flowing procedures. First, the initial height and initial mass of the frost layer were measured after the cold brine was removed from the pipe on which the frost layer was developed. After that, the pipe was set in the experimental apparatus, and the jet flow, whose temperature and humidity were controlled, was blown against the pipe. To obtain data of the amount of sublimation from the frost layer, the jet flow was stopped after a certain time interval, and the mass of the test pipe was measured by means of two electric balances (measurement accuracy 1 mg). Considering the correction of the balances and the measurement accuracy, the uncer-

tainty for the amount of sublimation was estimated to be within approximately ±1 mg.

The experimental data were obtained under the following conditions. Ratio of distance between nozzle and frost surface, $H/B=2 \sim 20$, jet flow temperature at nozzle outlet $T_\infty=272.2 \sim 268.2$ K, relative humidity of jet flow $\phi_\infty=30 \sim 80\%$, jet flow velocity at nozzle outlet $U_B=5 \sim 25$ m/s, initial frost height $H_f=1.0 \sim 7.0$ mm, and initial frost density $\rho_f=60 \sim 150$ kg/m^3.

4. Experimental Results and Discussion

4.1 Sublimation characteristics from frost layer

The frost layer has a rough surface and a density distribution as shown in Fig. 3. Therefore, the actual sublimation area is larger than the apparent surface area, and the defrosting characteristics are influenced by this fact[4)-6)].

Figure 4 indicates photographs of the morphology of the frost layer and sketches of the flow behavior around the pipe during sublimation by the impinging jet flow. The morphology of the frost layer was observed using a digital video recorder. On the other hand, the flow visualization around the pipe was carried out by means of the tuft screen method with the digital video recorder. A thread of 0.01 mm diameter and 18 mm length bonded to a needle (diameter: 0.5 mm, length 33 mm) was used as the tuft. Sixteen tufts were set around the pipe at intervals of 45 deg in the pipe circumferential direction and the pipe vertical direction. These data were obtained under the conditions of ratio of distance between nozzle and frost surface, $H/B=10$, jet flow velocity at nozzle outlet $U_B=20$ m/s, relative humidity of jet flow $\phi_\infty=50\%$, jet flow temperature at nozzle outlet $T_\infty=268.2$ K, initial frost height $H_f=6.0$ mm, and initial frost density $\rho_f=110$ kg/m^3. Here, the air flowed from the upper side to the lower side in Fig. 4.

The thickness of the frost layer at the stagnation point 10 min after starting the test run (Fig. 4(b)) decreases markedly compared with that of the initial shape (Fig. 4(a)). This fact can be considered to be because the mass transfer coefficient is extraordinarily high at the stagnation point of the impinging jet flow. In addition, the jet flows to the inside of the frost layer, because it has a dendritic crystal structure, therefore the actual area for mass transfer increases. By reducing the thickness of the frost layer, it is observed that the flow around the pipe separates from the upper side of the frost layer. For the case of a 20 min time lapse (Fig. 4(c)), the upper part of the pipe is exposed, and the jet flows horizontally along the pipe surface and separates from the pipe. In addition, at $t=80$ min (Fig. 4(d)), the frost layer disappears

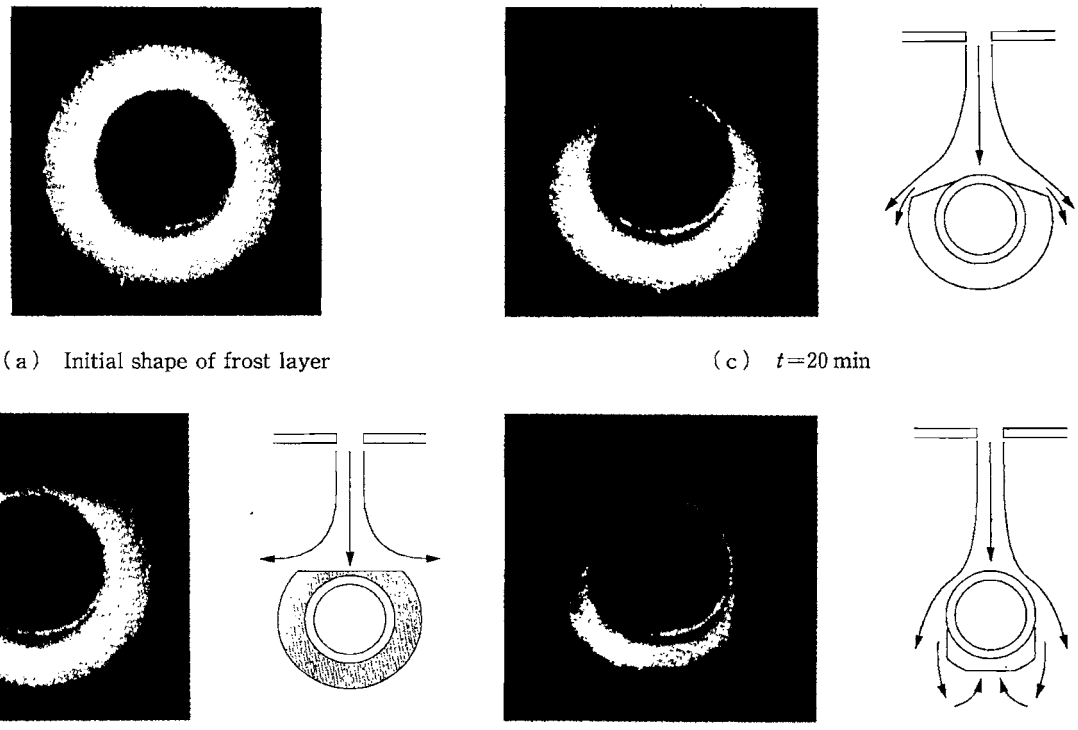

(a) Initial shape of frost layer

(c) $t=20$ min

(b) $t=10$ min

(d) $t=80$ min

Fig. 4 Shape of the frost layer and air flow pattern

from 60% of the pipe surface area except for the lower part of the pipe. When the frost layer has the morphology shown Fig. 4(d), vortices behind the pipe are observed. Finally, all of the frost layer is removed from the pipe within the time of 164 min for the present experiment.

4.2 Time histories of the sublimation from a frost layer

Figure 5 presents time histories of the mass of the frost layer M_f, jet flow temperature at the nozzle outlet T_∞, and mean temperature of the pipe surface T_p under the same conditions as shown in Fig. 4. Here, T_p denotes mean temperature calculated for upper, lower, right, and left parts of the pipe surface. At the beginning of the defrosting process, the mass of the frost layer decreases rapidly, since the upper part of the frost layer is defrosted as mentioned above. As time elapses, the amount of defrosting decreases due to the reduction in surface roughness and the separation of the jet flow from the pipe, according to the changing shape of the frost layer. On the other hand, T_p drops quickly from the beginning of the experiment because of the sublimation from the frost layer with an endothermic reaction. After 30 min, however, T_p increases with time. This can be explained by the fact that the amount of defrosting decreases as time passes, and the impinging jet flow contacts directly the exposed pipe at the stagnation point. Therefore, the pipe surface temperature approaches the jet flow temperature at the nozzle outlet.

4.3 Temperature distribution in a frost layer

Since the frost layer has a dendritic crystal structure, the sublimation also occurs from the inside of the frost layer, therefore it is expected that defrosting can be promoted. In the present experiments, the temperature distribution in the frost layer was measured to determine the sublimation characteristics of the frost layer.

Figure 6 indicates some measurement points in the frost layer. As shown in the figure, four T-type thermocouples of 0.1 mm diameter were set at vertical intervals of 2.0 mm above the stagnation point ($\theta=0$ deg) of the pipe. The defrosting experiments were carried out by means of the pipe on which the frost layer was developed.

Figure 7 shows the vertical temperature distribution in the frost layer at the stagnation point. The experiment was performed under the following conditions: $H/B=10$, jet flow velocity at nozzle outlet $U_B=5$ m/s, initial frost height $H_f=6.0$ mm, relative humidity of jet flow $\phi_\infty=70\%$, jet flow temperature at nozzle outlet $T_\infty=268.2$ K, and initial frost density $\rho_f=110$

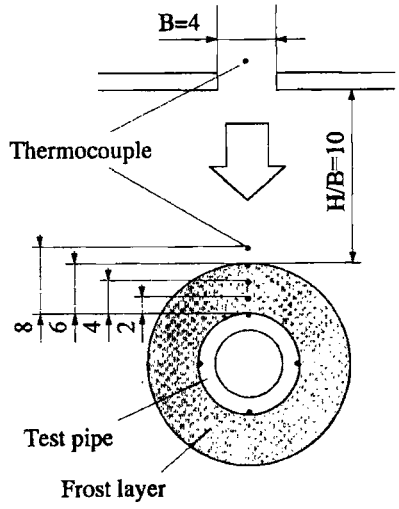

Fig. 6 Details of test pipe for measuring temperature distribution in a frost layer

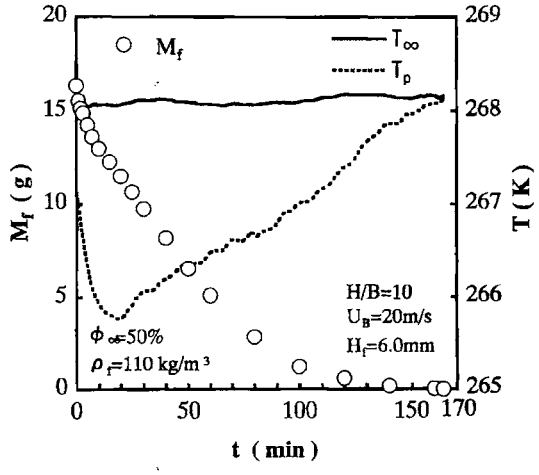

Fig. 5 Time history of temperature and M_f

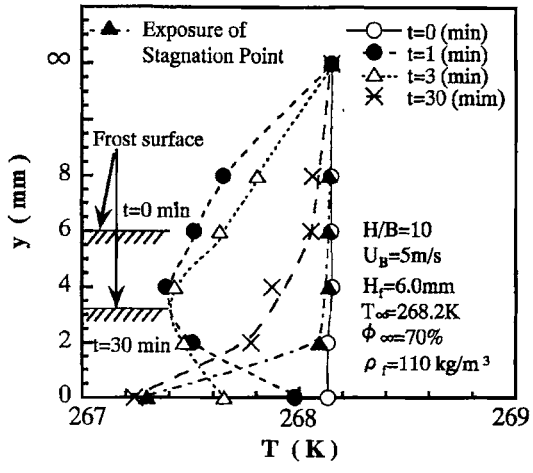

Fig. 7 Vertical temperature distribution in a frost layer

kg/m^3. In the figure, the ordinate denotes the vertical position from the pipe surface, and the horizontal lines and oblique lines denote the top of the frost layer at $t=0$ min and 30 min, respectively.

It is seen from the figure that the frost layer temperature drops by 1.5 K at 1 min after the experiment begins. In addition, as the result of the fact that the temperature near the pipe surface decreases with time, it is understood that the sublimation occurs in the frost layer. For the 30 min time lapse, an increase in temperature near the frost layer surface is observed. This increase is explained by the fact that the convection heat is supplied from the jet flow to the surface of the frost layer. On the other hand, the pipe surface temperature at the stagnation point remains at a low value even after the pipe surface is exposed to the moist air. The fact may result from the endothermic reaction of the frost layer around the stagnation point.

4.4 Time histories of thermal energy balance of a frost layer

In these experiments, most heat for the sublimation is supplied by the convection heat transfer from the jet flow. Therefore, the energy balance between the jet flow and the frost layer was investigated to determine the convection heat transfer. Quantity of convection heat Q_{cv} was estimated by calculation of the energy balance around the frost layer by the following equation.

$$Q_{cv}=Q_s+Q_f+Q_p \quad (1)$$

Where, Q_s, Q_f, and Q_p denote the amount of sublimated latent heat, sensible heat of frost layer, and sensible heat of test pipe, respectively at a particular time interval. They are defined as follows.

$$Q_s=L\cdot\Delta M_s \quad (2)$$

$$Q_f=M_f C_{pf}\Delta T_f \quad (3)$$

$$Q_p=M_p C_{pp}\Delta T_p \quad (4)$$

Here, ΔM_s is the amount of sublimation from the frost layer at that time interval, L is sublimate latent heat of ice, ΔT_f, ΔT_p, C_{pf}, and C_{pp} are temperature difference at that time interval and specific heat of the frost layer and the test pipe, respectively.

Figure 8 shows time histories of the thermal energy balance around the frost layer under the same conditions as indicated in Fig. 6. As shown in Fig. 8, the amounts of sensible heat of both the frost layer Q_f and the test pipe Q_p are very small (2 ~ 3%) compared to the convection heat Q_{cv}. Thus, it is noted that most of the supplied heat by the convection is provided to the ice sublimation of the frost layer. At the beginning of the experiment, the convection heat Q_{cv} shows a large value because the frost layer still has a large height and actual sublimation area. After that, Q_{cv} decreases gradually with time. This tendency can be explained by the fact that the surface area of the frost layer decreases due to the exposure of the pipe surface, and the area, in which the impinging jet flow can contact directly, also decreases with time because of the separation from the frost layer.

4.5 Mass transfer of frost sublimation

In the present experiments, the sublimation characteristics are classified in two periods during defrosting by the impinging jet flow. The first period is defined from the beginning of defrosting to the time when the frost layer at the stagnation point is removed by sublimation and the pipe surface is exposed to the air flow. The second period is denoted as starting after the first period and continuing until the completion of defrosting. For the latter case, defrosting shows markedly complicated phenomena because of a decrease in the sublimation area of the frost layer with time. Thus, in the present study, the experimental data are classified into the two periods mentioned above for analyzing the sublimation characteristics. Here, subscripts (0) and (c) denote time average from the beginning of the experiment until the stagnation point of the pipe surface is exposed (first period), and time average after the first period until the completion of defrost (second period), respectively.

The mean Sherwood number is defined as the following equation for both periods.

$$Sh=\frac{h_D\cdot d_f}{D}=\frac{m_{Af}(d+2H_f)}{(C_s-C_\infty)D} \quad (5)$$

Where, m_{Af} is mean mass flux of sublimation, C_∞ is water-vapor mass concentration of jet flow, and C_s is saturated water-vapor mass concentration of air at the frost layer temperature. For calculating m_{Af}, the

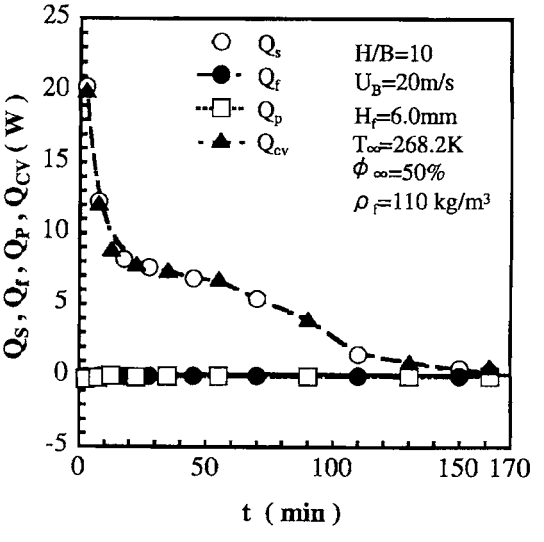

Fig. 8 Time history of Q

projectional area of the frost layer was adopted as the apparent surface area of the frost layer. In addition, D is diffusion coefficient of air, and d_f is the representative length ($d_f=d+2H_f$).

Figure 9 demonstrates the effect of the jet flow velocity at the nozzle outlet on mass transfer. The ordinate denotes mean Sherwood number Sh, while the abscissa denotes Reynolds number Re_B based on the velocity at nozzle outlet U_B and width of nozzle B. Re_B is defined by the following equation.

$$Re_B=\frac{U_B\cdot B}{\nu} \qquad (6)$$

As indicated in Fig. 9, Sh_c shows a larger value compared to that of sublimation from naphthalene[2] by 20 ~ 50%. This increase in Sh_c is explained by the fact that the surface roughness of the frost layer causes the actual sublimation area to enlarge. In addition, it is seen that the rate of increase of Sh_c in the present experiment is greater than that of the sublimation from the naphthalene. The frost layer has a dendritic crystal structure with density distribution as shown in Fig. 3. Therefore, for the case of large Re_B, an air flow may exist in the frost layer near the pipe surface, at which density is large as mentioned above, so sublimation should also be promoted.

Figure 10 indicates the relationship between mean Sherwood number Sh and density ratio ρ^* to show the effect of initial frost density on the mass transfer of the frost layer. The density ratio ρ^* is defined as

$$\rho^*=\frac{\rho_f}{\rho_{ice}} \qquad (7)$$

Here, ρ_{ice} is density of ice at 0°C.

It is noted from the figure that Sh decreases with an increase in ρ^*. It is assumed that it is difficult for the jet flow to enter the frost layer inside in the event that ice particles of the frost layer exist close to each other and as a result, the actual sublimation area decreases.

The effects of initial frost height H_f on mass transfer until the exposure of stagnation point (first period) and until the completion of defrosting (second period) are shown in Figs. 11 and 12, respectively. The abscissa shows the ratio of initial frost layer height to the representative length H_f/d_f. As shown in Fig. 11, Sh_0 increases monotonically with increasing H_f/d_f for the time period until the occurrence of the stagnation point. The increasing Sh_0 is caused by the fact that the actual sublimation area increases with an increase in H_f/d_f, furthermore there is little shape change of the frost layer by the sublimation for this time period. On the other hand, the results in Fig. 12 show that Sh_c decreases gradually with an increase in H_f/d_f until the completion of the defrosting. As H_f/d_f increases for the second period, the shape of the frost layer varies markedly with time elapsed and the jet flow separates from the frost layer. As a result, the amount of sublimation decreases with time.

Figure 13 presents the relationship between Sh and H/B. It is understood that Sh decreases with increasing H/B. The fact is explained as follows. With increasing H/B, the jet flow attainment velocity decreases at the impinging point on the pipe. In addition, the flow pattern of jet flow varies from the potential core region and passes through the transition region to the fully developed jet region. On the other hand, it is noted that the effect of H/B on Sh_c, which is the mean Sherwood number during the time period from exposure of stagnation point to completion of defrosting, is less than that on Sh_0 from the

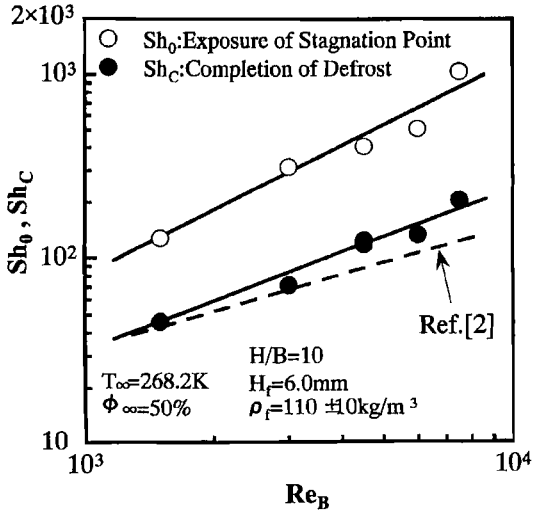

Fig. 9 Relationship between Sh and Re_B

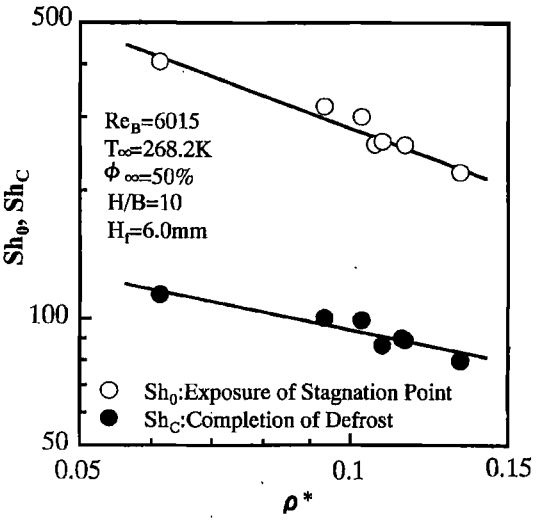

Fig. 10 Relationship between Sh and ρ^*

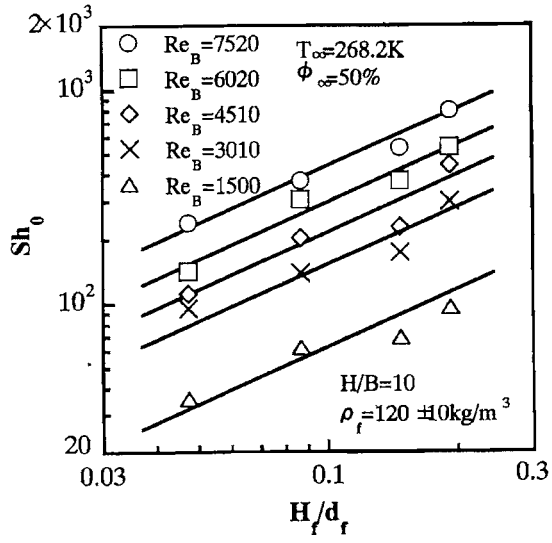

Fig. 11 Relationship between Sh_0 and H_f/d_f

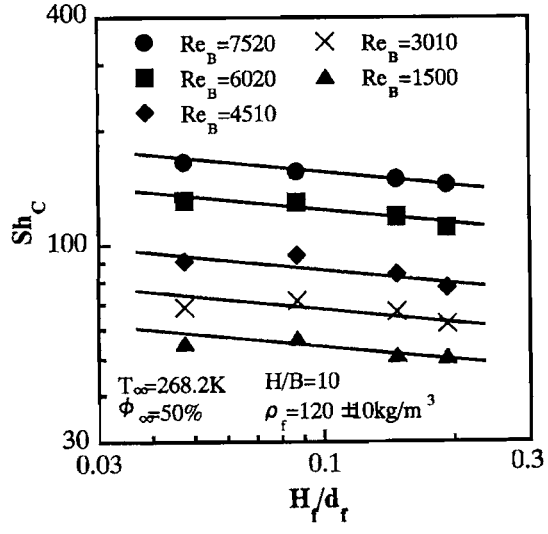

Fig. 12 Relationship between Sh_c and H_f/d_f

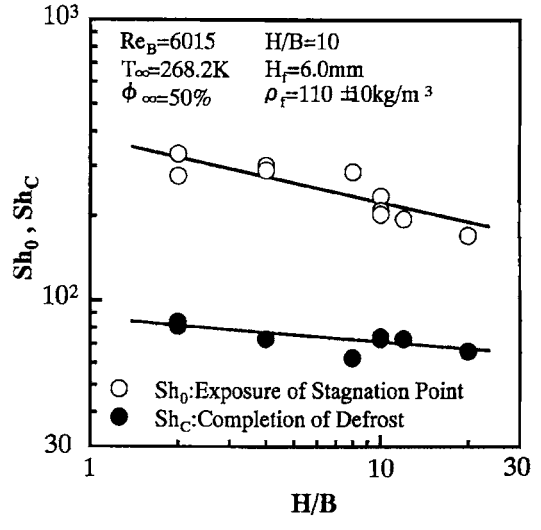

Fig. 13 Relationship between Sh and H/B

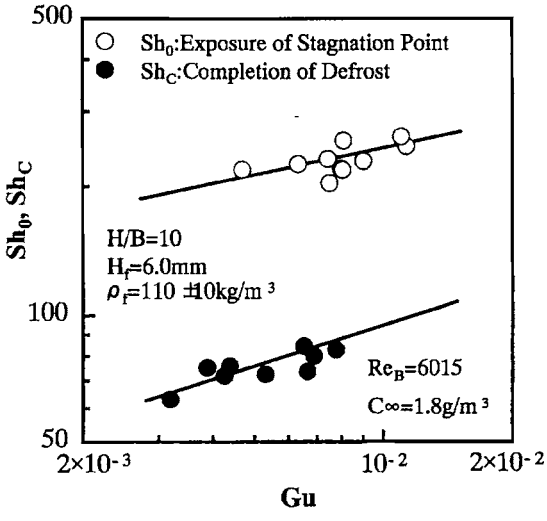

Fig. 14 Relationship between Sh and Gu

beginning to the exposure of the stagnation point. When H/B is large, the jet flow spreads widely until it reaches the frost layer surface, therefore the sublimation is promoted over the entire surface of the frost layer, while the attainment velocity of the jet flow decreases at the impinging point on the pipe. It is assumed that these two effects on the mass transfer compensate each other for the case of Sh_c.

In general, it is difficult to precisely estimate the frost surface temperature during defrosting because the frost layer has a dendritic crystal structure and the surface temperature does not remain constant due to sublimation from the frost layer inside. Therefore, in the present study, Guman number Gu was adopted as a non-dimensional parameter based on both the attainment temperature of the jet flow at the impinging point on the pipe and the mean pipe surface temperature to obtain the representative temperature of frost layer surface as reported in Ref.(8). Guman number can be regarded as the ratio of heat transfer in the frost layer to that of the jet flow.

$$Gu=\frac{T_a-T_P}{T_a} \qquad (8)$$

Here, T_a is the attainment temperature of the jet flow at the stagnation point obtained by estimating the temperature distribution as shown in Fig. 6. Figure 14 indicates the effect of T_a on mass transfer using mean Sherwood number Sh and Guman number Gu. Sh increases with an increase in Gu as indicated in Fig. 14. The saturated water-vapor mass concentra-

tion of the frost layer is affected by T_a, therefore the driving force of mass transfer from the frost layer rises between the jet flow and the frost layer with increasing T_a.

Based on the effects of these parameters on Sh_0 and Sh_c, the following correlation equations were derived by the root-mean square method with standard deviations of ±14.0% and ±9.8%, respectively.

$$Sh_0=3.68\times10^{-2}Re_B^{1.16}\rho^{*-0.79}\times(H_f/d_f)^{0.89}(H/B)^{-0.23}Gu^{0.20}Sc^{1/3} \quad (9)$$

$$Sh_c=7.38\times10^{-2}Re_B^{0.90}\rho^{*-0.41}\times(H_f/d_f)^{-0.12}(H/B)^{-0.09}Gu^{0.31}Sc^{1/3} \quad (10)$$

Here, the exponent of Schmidt number Sc was adopted to be 1/3 according to conventional experimental results.

5. Conclusions

An experimental study was carried out to determine the sublimation characteristics from the annular frost layer developed on a pipe exposed to an impinging jet flow using the frost sublimation phenomenon. The effects of some parameters on sublimation characteristics were clarified as follows.

(1) Morphology of the frost layer and the behavior of jet flow around the frost layer were observed during the sublimation process from the annular frost layer developed on a pipe exposed to an impinging jet flow. As a result, it was found that the jet flow around the frost layer was greatly affected by the morphology of the frost layer.

(2) By measuring the temperature distribution in the frost layer during sublimation, it was clarified that sublimation also occurred in the frost layer owing to the obtained data which showed a decrease in temperature with time elapsed.

(3) The effects of sublimation parameters on the time histories of both mass and thermal energy balance of the frost layer were determined.

(4) The non-dimensional correlation equations of mass transfer of defrosting were derived as functions of various parameters such as jet flow velocity at nozzle outlet, water-vapor mass concentration of jet flow, attainment temperature of jet flow, initial density of frost layer, initial frost height, and distance between nozzle and frost layer surface.

References

(1) Sugawara, M. et al., Trans. Jpn. Soc. Mech. Eng., (in Japanese), Vol. 56, No. 531, B (1990), p. 3457.

(2) Kumada, M. et al., Trans. Jpn. Soc. Mech. Eng., (in Japanese), Vol. 38, No. 315, B (1972), p. 2915.

(3) Kochs, M., Int. J. Heat and Mass Transfer, Vol. 36, No. 7 (1993), p. 1727.

(4) Inaba, H. and Imai, S., Trans. Jpn. Soc. Mech. Eng., (in Japanese), Vol. 61, No. 585, B (1995), p. 1818.

(5) Inaba, H. and Imai, S., Trans. Jpn. Soc. Mech. Eng., (in Japanese), Vol. 61, No. 586, B (1995), p. 2261.

(6) Inaba, H. and Imai, S., Trans. Jpn. Soc. Mech. Eng., (in Japanese), Vol. 63, No. 585, B (1997), p. 1000.

(7) Inaba, H. et al., Proceedings of 33rd National Heat Transfer Symposium of Japan, (1996), p. 535.

(8) Smolsky, B.M. and Sergeyev, G.T., Int. J. Heat and Mass Transfer, Vol. 5 (1962), p. 1011.